Conceptual Aircraft Design Based on a Multiconstraint Genetic Optimizer

Luciano Blasi,* Luigi Iuspa,† and Giuseppe Del Core‡
Second University of Naples, 81031 Aversa, Italy

Introduction

IN the last years genetic algorithms (GAs) have received much attention as a powerful design tool in many areas of aerospace engineering. These probabilistic-type methods, based on the principle of the natural evolution, have shown their effectiveness and robustness in a wide range of optimization problems.[1–5] Compared with classical deterministic approaches, GAs' superior effectiveness in performing optimization tasks is mainly from some specific features such as the capability to handle simultaneously continuous integer and discrete design variables, a parallel-like searching method leading to a greater effectiveness in finding global minimum within the design space. Moreover, as genetic-type optimization is guided only by a function of merit (or fitness) value, no mathematical information on the objective function is required. Therefore function discontinuities can be easily managed. In this Note an application in the field of aircraft conceptual design is described. A genetic optimizer has been coupled with a sizing code to define a short/medium range preliminary aircraft configuration, powered by turbofan engines, fully compliant with given requirements and allowing minimum direct operating cost. Parametric formulas[6–8] have been used for aerodynamics, weights, and low-speed performance calculation. Rationale for GA application in conceptual design with reference to selection and sizing is well presented in Ref. 9. Other relevant examples of genetic approach in aircraft design are reported in Refs. 10–13.

Optimization Process Definition

Specific genetic-oriented parameters and operators have been chosen, together with a proper design space and design requirements set definition.

Fitness Function

Because GAs are structured to promote the best individuals, to minimize direct operating cost (DOC) the following fitness function has been defined for each ith individual:

$$\mathrm{fit}_i = \mathrm{DOC}_{\max} - \mathrm{DOC}_i \tag{1}$$

where $\mathrm{DOC}_{\max}$ is a constant value great enough to avoid negative fitness values. In this work a value of 10 (c\$/pax/n mile) has been set for $\mathrm{DOC}_{\max}$. A detailed description of the method used for DOCs calculation can be found in Ref. 14.

Penalty Functions

As well known by users of GA, a constrained optimization problem is treated as an unconstrained one by using proper penalty functions that degrade fitness value in relation to the degree of constraints violation. Let S_r be the value of a generic constraint function, $S_r^{\min} - S_r^{\max}$ its allowable range, and P the total number of constraint functions. The penalized fitness fit_i^*, related to the ith individual, has been calculated as follows:

$$\mathrm{fit}_i^* = \frac{\mathrm{fit}_i}{\prod_{r=1}^{P} K_r} \tag{2}$$

where

$$K_r = \begin{cases} \left[\dfrac{(S_r^{\max} - S_r)}{(S_r^{\max} - S_r^{\min})}\right]^{q_r} & (S_r < S_r^{\min}) \\ 1 & (S_r^{\min} \le S_r \le S_r^{\max}) \\ \left[\dfrac{(S_r - S_r^{\min})}{(S_r^{\max} - S_r^{\min})}\right]^{q_r} & (S_r > S_r^{\max}) \end{cases} \tag{3}$$

Table 1 Constraint functions parameters

Constraint function, units	Min	Max	Exp
Rate of climb at cruise altitude	300	10,000	2
Balanced field length, ft	0	5,500	2
Landing field length, ft	0	4,500	2
Approach speed, kn	0	130	2
Cruise range/design range	0.5	1.0	2
Second segment climb gradient	0.024	0.30	2
Mission fuel/max fuel capacity	0	1.0	2
Wing tip chord, ft	3.3	13	2

To avoid a premature convergence to a suboptimal solution, the penalized fitness has been further scaled using a linear model.[15] Exponent values as well as the allowable range defined for each constraint functions have been summarized in Table 1. Cruise range/design range constraint has been introduced just to avoid an unrealistic mission profile shape (at least 50% of design range should be covered in cruise) when cruise altitude is changed during the optimization process. Wing-tip-chord constraint has been introduced in order to limit tip-chord minimum length when wing taper ratio is changed, thus preserving sufficient space for systems installation (e.g., aileron actuators).

Genetic Operators

Couples of individuals have been selected for mating through a roulette-wheel criterion. Offspring have been generated applying a single-cut crossover. Finally a 0.04 bitwise mutation rate has been applied to the new individuals. However, by varying mutation probability value in the range 0.01–0.04, negligible differences in the final results have been observed. A detailed description of GA operators just mentioned can be found in Ref. 15. Rather than to select a crossover probability, in this work a fixed number of couples has been set. Once crossover and mutation operators have been applied, all of the new individuals have been added to the current population. On the basis of the fitness value, the extended population that results has been sorted and trimmed by deleting the worst individuals. In this way a new population having always the same size has been obtained. Using this approach, the evolution process can take into account the genetic inheritance of all of the best individuals coming from the previous generations.

Design Variables

The selected design variables describing aircraft configuration have been summarized in Table 2. Their range/values and related binary strings length chosen to ensure a proper variable resolution can also be found. As for flap deflection and cruise altitude, the equivalent decimal value of their binary representation has been used to point a vector containing all of their actual values. As for number of abreast and engine location, a single variable, called *configuration index*, has been defined. Its equivalent decimal value is related to aircraft configuration as shown in Table 3. As can be noticed, wider binary substrings have been used to codify the discrete variables allowing to give them an higher probability to be changed when single-cut

Received 25 January 1998; revision received 15 August 1999; accepted for publication 6 September 1999.

*Research Assistant, Dipartimento di Ingegneria Aerospaziale, Via Roma, 29; lucblasi@unina.it.
†Ph.D. Graduate, Dipartimento di Ingegneria Aerospaziale, Via Roma, 29.
‡Associate Professor, Dipartimento di Ingegneria Aerospaziale, Via Roma, 29.

Table 2 Design variables

Variable, units	Range/values	String length bits
Wing sweep, deg	10–30	6
Wing t/c change	0–0.05	6
Wing area, ft^2	860–1400	7
Takeoff flap deflection, deg	0,10,15,20	6
Landing flap deflection, deg	25,30,35,40	6
Wing taper ratio	0.15–0.35	6
Wing aspect ratio	7–9.5	6
Configuration index	1,2,3,4	6
Engine thrust scaling factor	1.0–1.3	6
Cruise altitude, ft × 1000 (m × 1000)	29,30,31,32,33,34,35,36 (8.8,9.1,9.4,9.8,10.1,10.4, 10.7,11.0)	6

Table 3 Configuration index value to aircraft configuration relationship

Configuration index	Aircraft configuration
1	5 abreast, fuselage mounted engines
2	6 abreast, fuselage mounted engines
3	5 abreast, wing mounted engines
4	6 abreast, wing mounted engines

Table 4 Design constants

Parameter	Value
Flap chord/wing chord	0.30
Flap span/wing span	0.55
Slat chord/wing chord	0.15
Slat span/wing span	0.75
Aileron chord/wing chord	0.30
Aileron span/wing span	0.20
Takeoff slat deflection, deg	20
Landing slat deflection, deg	20
Engine number	2
Aisle number	1
Wing center section fuel tank	yes
Wing position	low

crossover and mutation operators have been applied. In this case the proper equivalent decimal value x_j^{cod} has been restored as follows:

$$x_j^{\mathrm{cod}} = \hat{x}_j^{\mathrm{cod}} - \mathrm{int}(\hat{x}_j^{\mathrm{cod}}/m_j)m_j \tag{4}$$

where $\hat{x}_j^{\mathrm{cod}}$ is the binary string oversampled equivalent decimal value and m_j is the number of the actual values assumed for the jth discrete variable. As far as wing arrangement is concerned, a trapezoidal straight tapered surface has been assumed with a linear thickness-to-chord (t/c) distribution between three fixed wing stations: 1) wing root, 2) wing kink, located at the 35% of semispan, and 3) wing tip. Wing t/c distribution has been changed adding the thickness-related design variable to the kink t/c reference value only. Root t/c and tip t/c have been computed as 130 and 90% of the kink t/c, respectively. According to these assumptions, the following wing t/c reference distribution has been assumed:

$$t/c(\mathrm{root/kink/tip}) = 0.139/0.107/0.096 \tag{5}$$

During the optimization process, the 14,000-lb (6229 daN)-reference engine thrust has been scaled keeping constant specific fuel consumption curves. The ratio between the installed thrust and the reference engine thrust (engine thrust scaling factor) has been used to scale reference engine weight linearly. In this work further potential design variables have been kept constant during the optimization process. They have been summarized in Table 4.

Design Requirements

Figure 1 shows the mission profile has been defined to estimate properly aircraft maximum takeoff weight. Maximum operating mach number (MMO) results from the aircraft maximum speed capability at the average cruise weight. Maximum operating speed has been fixed to achieve MMO at 23,000-ft (7010 m) altitude. The complete set of mission requirements has been summarized in Table 5.

Optimization Process Final Results

No convergence criteria have been used. Once the 40th generation has been analyzed, the process is automatically stopped. Forty different couples have been selected from a basic population of 80 individuals and mated to generate 80 new offspring. Being GA, a probabilistic guided-search method, to obtain a more reliable result five

Table 5 Mission requirements

Mission parameter	Required value
Passengers number	110
Design range	1600 n miles
Reserves	45 min extended cruise + 100 n miles alternate
Cruise speed	Not specified
Cabin altitude at cruise altitude	5000 ft
Balanced field length	5500 ft at max takeoff weight
Landing field length	4500 ft at max landing weight
Approach speed	≤ 130 kn

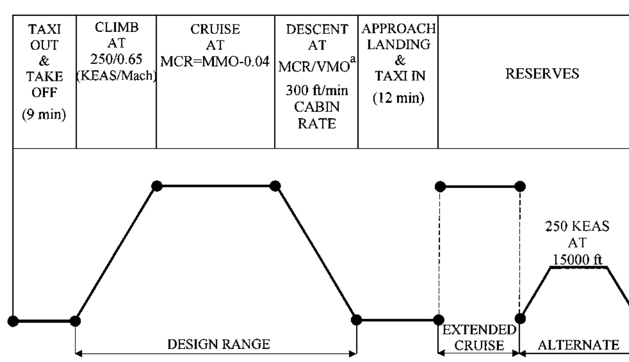

[a] 250 KEAS constant speed below 10000 ft

Fig. 1 Mission profile.

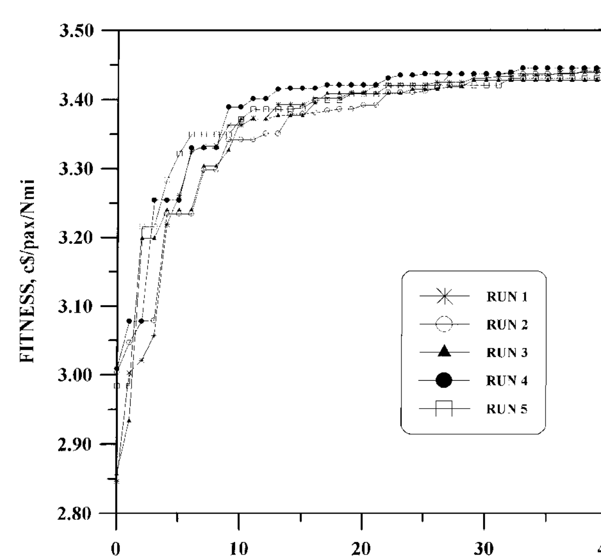

Fig. 2 Best fitness evolution over five runs ($\mathrm{DOC_{max}} - \mathrm{DOC}$).

Table 6 Optimized configurations main data

Aircraft main data, units	Run 1	Run 2	Run 3	Run 4	Run 5	Refined
Wing sweep, deg	19.0	20.8	19.0	21.4	20.0	21.4
Wing t/c change	0.0024	0.0	0.0016	0.0	0.0	0.0
Wing area, ft^2	966.6	966.6	954.8	970.9	970.9	966.6
Wing taper ratio	0.299	0.242	0.251	0.270	0.251	0.274
Wing aspect ratio	9.50	9.46	9.22	9.46	9.42	9.46
Installed thrust per engine, lb	16,930	17,330	17,530	17,200	17,390	17,330
(Engine thrust scaling factor)	(1.209)	(1.238)	(1.252)	(1.228)	(1.242)	(1.238)
Max Takeoff weight, lb	100,127	100,560	100,562	100,559	101,025	100,652
Cruise Mach number	0.748	0.755	0.753	0.755	0.756	0.757
Cruise altitude, ft	34,000	35,000	34,000	35,000	34,000	35,000
Mission fuel/max fuel capacity	0.996	0.980	0.996	0.989	0.993	0.999
Balanced field length, ft	5,500	5,478	5,474	5,498	5,465	5,492
Landing field length, ft	4,373	4,424	4,425	4,365	4,346	4,380
Second segment climb gradient	0.0245	0.0268	0.0260	0.0261	0.0264	0.0268
Takeoff flap deflection, deg	15	15	15	15	15	15
Landing flap deflection, deg	35	35	35	40	40	40
Configuration index	3	3	3	3	3	3
Fitness value, c$/pax/n mile	3.440	3.441	3.428	3.444	3.433	3.451

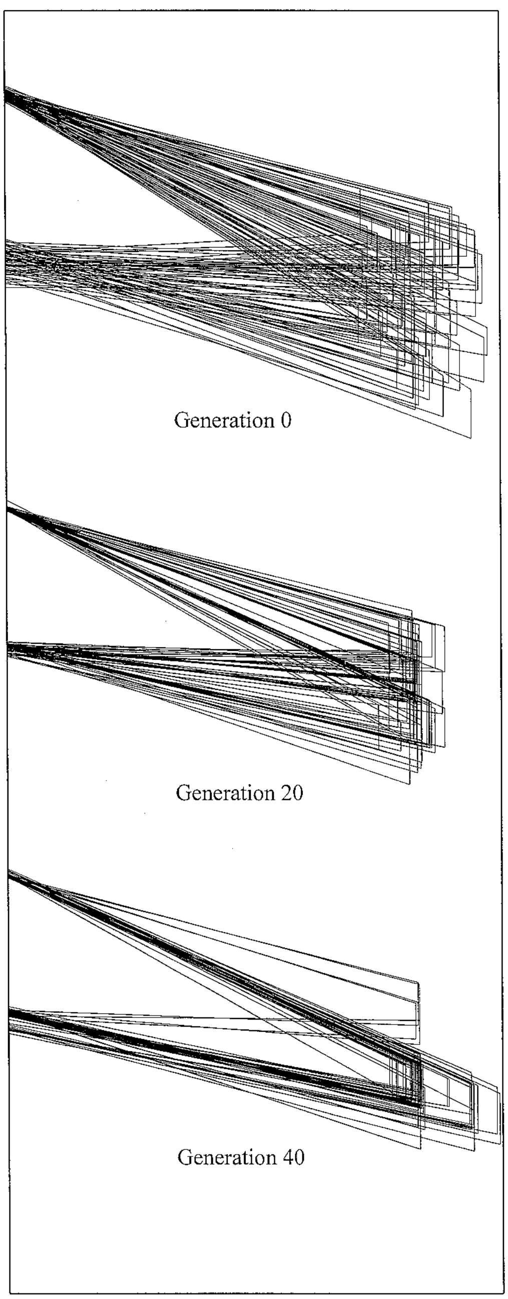

Fig. 3 Right-half-wing superposition at generation 0, 20, and 40.

optimization tasks have been performed, each related to a different starting population. The optimized configurations' main characteristics have been summarized in Table 6. To verify if a further design solution improvement could be obtained, a restarting of the optimization process has been performed. The optimized configurations (Run 1–5) have been used as predefined individuals of a new randomly generated population. The result is shown in the last column of Table 6. As can be seen, no significant improvement has been obtained, the refined solution having negligible differences compared with the earlier ones. Although GA has not been able to provide a single solution, nevertheless its capability to identify the most promising area within the design domain is quite clear. Moreover, the selected generation number has allowed a satisfactory development of the population, in fact no premature convergence has been observed (Fig. 2). Wing planform evolution is shown in Fig. 3 by population right-half wing superposition at generations 0, 20, and 40. Whereas the starting randomly generated population exhibits the widest variety of wing planform, final generation (40) still retains some differences among wing planform; this is a further confirmation that no premature convergence has occurred in the optimization process.

Conclusions

Final results have confirmed GA effectiveness to explore the design domain as well as its capability to identify the most promising design variables set. Moreover GA capability to easily handle both continuous and discrete variables gives the genetic optimization procedure high flexibility in aircraft configuration and mission profile modeling. All of these features make GA a very attractive tool to perform aircraft configuration selection and sizing in the early phase of the design process when aircraft main characteristics are requested to be identified.

References

[1] Altus, S. S., Kroo, I. M., and Gage, P., "A Genetic Algorithm for Scheduling and Decomposition of Multidisciplinary Design Problem," American Society of Mechanical Engineers, Paper 95-141, Sept. 1995.

[2] Vicini, A., and Quagliarella, D., "Inverse and Direct Airfoil Design Using a Multiobjective Genetic Algorithm," *AIAA Journal*, Vol. 35, No. 9, 1997, pp. 1499–1505.

[3] Obayashi, S., Yamaguchi, Y., and Nakamura, T., "Multiobjective Genetic Algorithm for Multidisciplinary Design of Transonic Wing Planform," *Journal of Aircraft*, Vol. 34, No. 5, 1997, pp. 690–693.

[4] Gage, P. J., Kroo, I. M., and Sobieski, I. P., "Variable-Complexity Genetic Algorithm for Topological Design," *AIAA Journal*, Vol. 33, No. 11, 1995, pp. 2212–2217.

[5] Ryan, G. W., "A Genetic Search Technique for Identification of Aircraft Departures," NASA CR 4688, Aug. 1995.

[6] Roskam, J., *Airplane Design—Pts I-VII*, Roskam Aviation and Engineering Corp., Kansas, 1988.

[7]Torenbeek, E., *Synthesis of Subsonic Airplane Design*, Delft Univ. Press, Kluwer Academic, Norwell, MA, 1982, pp. 167–170, 263–294, 445–465, 487–556.

[8]Raymer, D. P., *Aircraft Design: A Conceptual Approach*, AIAA Education Series, AIAA, Washington, DC, 1989, pp. 391–405.

[9]Crossley, W. A., and Laananen, D. H., "Conceptual Design of Helicopters via Genetic Algorithm," *Journal of Aircraft*, Vol. 33, No. 6, 1996, pp. 1062–1070.

[10]Crispin, Y., "Adaptive Conceptual Optimization of General Aviation Aircraft," AIAA Paper 92-4195, Aug. 1992.

[11]Crispin, Y., "Aircraft Conceptual Optimization using Simulated Evolution," AIAA Paper 94-0092, Jan. 1994.

[12]Bramlette, M. F., and Cusic, R., "A Comparative Evaluation of Search Methods Applied to Parametric Design of Aircraft," *Proceedings of the 3rd International Conference on Genetic Algorithms*, Morgan Kaufmann, San Mateo, CA, 1989, pp. 213–238.

[13]Roth, G. L., and Crossley, W. A., "Conceptual Design of a Commercial Transport Aircraft Using a Genetic Algorithm-Based Approach," AIAA Paper 98-4934, Sept. 1998.

[14]Roskam, J., *Airplane Design—Part VIII*, Roskam Aviation and Engineering Corp., Kansas, 1988, Chap. 5, pp. 80–109.

[15]Goldberg, D. E., *Genetic Algorithms in Search, Optimization and Machine Learning*, Addison Wesley Longman, Reading, MA, 1989, pp. 59–88.

Numerical Evaluation of Airfoil Friction Drag

Giovanni Lombardi,* Maria Vittoria Salvetti,† and Dario Pinelli‡
University of Pisa, 56126 Pisa, Italy

Introduction

THE prediction of friction drag is of significant importance in the design of aerodynamic configurations, especially in aircraft design. Unfortunately, this is traditionally a difficult task, both experimentally and numerically. In experiments, it is difficult to reproduce all of the features of the physical problem, for example, the Reynolds number. Moreover, problems arise due to interference effects, in particular with the model support, and due to the difficulty in measuring quantities that are small compared to the others involved in the tests. From the numerical point of view, in the past only potential flow solvers were available. Thus, predictions were substantially limited to the induced drag, and only attached flow conditions in subsonic or supersonic regimes could be analyzed.

The use of a boundary-layer model has been a powerful tool, for friction drag prediction, but it is limited to attached flows. The increase in computing performance has lead to the possibility of simulating more complex flows. At present, several commercial codes are available that discretize laminar and Reynolds-averaged Navier–Stokes equations (RANS). These codes are widely used to predict the pressure loads acting on bodies of different shapes and also on aerodynamic configurations. Examples of such applications can be found, for instance, in Refs. 1 and 2.

In principle, the RANS codes are able to predict both the pressure and friction components of drag. This approach seems very attractive because numerical analysis requires lower cost and less time to obtain results than experimental tests. However, although the capabilities of RANS codes are well stated for the evaluation of pressure distributions,[1] many problems still exist for the evaluation of the friction drag, which appears to be very sensitive to near-wall grid resolution and to the employed turbulence model.

In this Note the capabilities of a Navier–Stokes solver to predict the friction drag over an airfoil are studied. In particular, the sensitivity to the grid resolution and to different RANS closure models is investigated for three different Reynolds numbers.

Numerical Methods

The commercial code FLUENT 5.0 has been used for the numerical solution of RANS equations. Different turbulence models are available in the code. In particular, the standard k–ε,[3] Renormalization Group (RNG) k–ε,[4] and Reynolds stress[5] models are used in the present study. The numerical method is based on a finite volume formulation applicable to structured or unstructured solution-adaptive grids. The numerical inviscid fluxes are evaluated by Roe's flux-difference splitting. A second-order spatial accuracy is obtained by a Taylor series expansion in the evaluation of the variables at the cell faces. Steady solutions are obtained by time marching the equations with an explicit, multistage, Runge–Kutta scheme with multigrid convergence acceleration.

Unfortunately, no experimental results are available for the friction drag. Therefore, the results are compared with those obtained by a boundary-layer solution, coupled with a potential solver. Clearly, this limits the analysis to subsonic flows and low angles of attack. However, this is a necessary first step in the assessment of the Navier–Stokes solver capabilities and may also give indications as to the computational resources needed for friction drag prediction on more complex configurations of engineering interest.

For boundary-layer evaluation, the code BLOWS[6] was used. This code is based on the Thwaites method for the simulation of the laminar boundary layer and on the Head method for the turbulent one. The code is able to predict the transition from laminar to turbulent flow.

Results

The analysis has been carried out by simulating the flow around the NACA 0012 airfoil, at 0-degree angle of attack, for three different values of the Reynolds number.

The results of the code BLOWS, in terms of total drag, are compared with the experimental data from Ref. 7 in Table 1. The comparison shows that the code is able to correctly predict the drag in the analyzed conditions, and, therefore, the results for the friction drag can be assumed as a reference.

The values of the friction coefficient obtained by the RANS solver are reported in Table 2 for different grid resolutions. The results are obtained at a Reynolds number of 3×10^6 using the standard k–ε turbulence model. In all of the cases, the grid is unstructured, and the near-wall resolution is increased by prescribing the maximum allowable distance from the body of the first cell centroid, in terms of wall units, $y^+ = u_\tau y/\nu$, where u_τ is the friction velocity, y is the physical distance of the first centroid from the wall, and ν is the kinematic viscosity. Because a logarithmic wall law is used in FLUENT to compute the friction coefficient, the first grid cell near the body should be in the logarithmic region, that is, $y^+ > 30$. From Table 2, it can be seen that an acceptable convergence of the computed value of the friction drag coefficient is reached only for $y^+ \leq 38$. For $y^+ \leq 38$, the chord distribution of the local friction drag

Table 1 Comparison between experimental data and BLOWS code results[a]

Reynolds	$C_{d\,\text{total}} \times 10^3$ (Ref. 7)	$C_{d\,\text{total}} \times 10^3$	$C_F \times 10^3$
3×10^6	6.0	6.228	5.340
6×10^6	6.0	6.173	5.040
9×10^6	6.0	6.208	5.080

[a]C_d and C_F are the airfoil drag and friction coefficients, respectively.

Received 18 October 1999; revision received 30 November 1999; accepted for publication 2 December 1999.

*Assistant Professor, Department of Aerospace Engineering, Via Diotisalvi 2. Member AIAA.

†Assistant Professor, Department of Aerospace Engineering, Via Diotisalvi 2.

‡Graduate Student, Department of Aerospace Engineering, Via Diotisalvi 2.